Monitoring Corrosion in Sacrificial Anodes With Pulsed Eddy Current and Electromechanical Impedance: A Comparative Analysis

Durgesh Tamhane, Sauvik Banerjee, and Siddharth Tallur

***Abstract*—Measuring the extent of corrosion of sacrificial anodes used in cathodic protection systems would enable real-time monitoring of the efficacy and remaining useful life of the cathodic protection system. This article presents a comparison of the sensing capabilities of pulsed eddy current (PEC) and electromechanical impedance (EMI) based techniques for measuring extent of corrosion of zinc sacrificial anodes. Experiments were conducted with a lead zirconate titanate (PZT) transducer attached to the sacrificial anode as well as with a PEC probe placed in the vicinity of the sacrificial anode. Accelerated corrosion tests were performed on the anode and the corrosion was quantified by the root mean square deviation (RMSD) of the conductance spectra for the EMI based measurement and area under the curve (AUC) method for the pulsed eddy current based measurement. The experimental results show good agreement with finite element method (FEM) simulations. We report that the EMI method has large sensitivity to onset of corrosion in the anode, with sensitivity reducing nonlinearly over time due to delamination of corrosion by-products. In contrast, the PEC method shows excellent linearity over the entire duration of the accelerated corrosion experiment. A key insight from this work is that an effective monitoring strategy could combine the merits of both sensing mechanisms, with EMI used for identifying incipient corrosion and PEC used for tracking the extent of corrosion over the life of the sacrificial anode.**

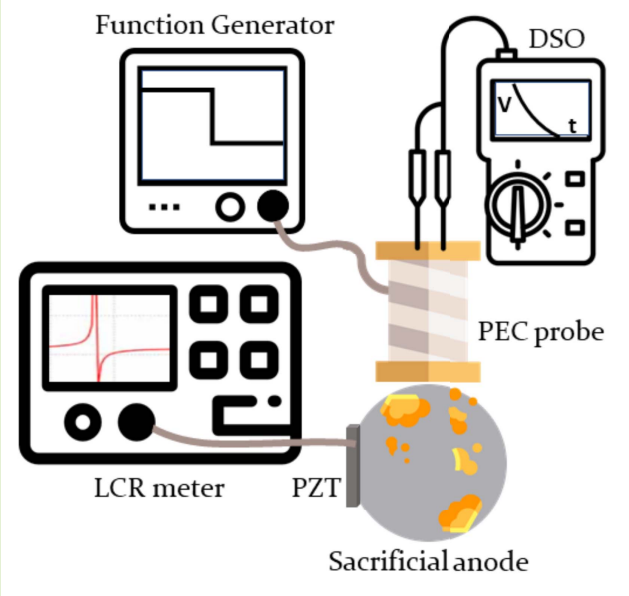

***Index Terms*—Structural health monitoring, corrosion, cathodic protection system, sacrificial anode, pulsed eddy current, electromechanical impedance.**

I. Introduction

DURABILITY of civil infrastructure is dependent on the strength of metals such as steel used in the construction of buildings, pipelines, and storage tanks, among other things. To protect these metals from corrosion, they are usually encased in insulated casings or covered with anti-corrosion coatings. Nonetheless, these metals are vulnerable to corrosion as soon as the substance in which they are embedded deteriorates, allowing corrosive chemicals to permeate and diffuse. The rate of corrosion is influenced by a variety of factors, including the quality of raw materials used in the preparation of concrete for reinforced steel structures, the air quality of the environment in which the structure is to be built, the water quality and salinity of marine infrastructure, etc. Installing a cathodic protection system is a simple and widely used method of protecting metals against corrosion [1], [2]. The cathodic protection system employs a sacrificial metal that is more electrochemically active (i.e. has a lower negative electrode potential) than the metal that is to be protected. Because it is more electrochemically active, the sacrificial anode is consumed by corrosion instead of the metal to which it is bonded, extending the service life of the infrastructure. To maintain effective corrosion protection, it is necessary to monitor the efficacy of a passive cathodic protection

Manuscript received January 20, 2022; revised February 25, 2022; accepted March 4, 2022. Date of publication March 8, 2022; date of current version April 14, 2022. This work was supported in part by IMPacting Research INnovation and Technology (IMPRINT)-2A administered by the Science and Engineering Research Board (SERB), Government of India, under Grant IMP/2018/001442; and in part by Sanrachana Structural Strengthening Pvt. Ltd., under Grant RD/0119-SSIMPQ2-001. The associate editor coordinating the review of this article and approving it for publication was Dr. Jürgen Kosel. *(Corresponding author: Siddharth Tallur.)*

Durgesh Tamhane and Siddharth Tallur are with the Department of Electrical Engineering, Indian Institute of Technology (IIT) Bombay, Mumbai 400076, India (e-mail: stallur@ee.iitb.ac.in).

Sauvik Banerjee is with the Department of Civil Engineering, Indian Institute of Technology (IIT) Bombay, Mumbai 400076, India (e-mail: sauvik@civil.iitb.ac.in).

Digital Object Identifier 10.1109/JSEN.2022.3157646

system. Direct monitoring methods include half-cell potential measurement [3], open-circuit potential test [4], DC current density measurement [5] etc. These tests necessitate the use of a three-electrode apparatus as well as the detachment of the sacrificial anodes from the cathodic protection system for several hours, obstructing their functionality.

Recently, we reported a method for monitoring extent of corrosion in sacrificial zinc anodes using electromechanical impedance (EMI) measurements obtained with lead zirconate titanate (PZT) transducers fitted on the anodes [6]. This method has also been employed for structural health monitoring of concrete structures, including monitoring of chlorine infiltration and carbonation of concrete [7]–[11]. The shift in resonance frequency with increasing degree of corrosion in zinc anodes exhibits large nonlinearity due to partial delamination of the corrosion product (zinc oxide) from the disc [6]. Estimation of the extent of corrosion of the sacrificial anode thus requires robust mathematical model and calibration of the corrosion and delamination mechanism to accurately capture the nonlinearity, or the use of multiple resonances to estimate extent of corrosion through graphical method [12], [13]. Measuring the shift in resonance frequency is suitable when the system under test experiences negligible mechanical damping. However, when there are sources of damping present in the system, peak frequency measurements are unreliable. For such systems, root mean square deviation (RMSD) of the EMI signature has been shown to be a reliable indicator of change in structural parameters in literature. Tawie *et al.* [14] and Ghafari *et al.* [15] validated the feasibility of the RMSD index for the evaluation of concrete and mortar properties. Moreover, Talakokula *et al.* [16] have demonstrated that the RMSD can also be applied as a damage index for detecting corrosion of rebars embedded in concrete.

Apart from EMI techniques, pulsed eddy current (PEC) and other electromagnetic methods are promising non-invasive corrosion detection approaches [17]–[22]. Using a time-varying magnetic field produced by an electromagnetic excitation coil, the PEC method generates eddy currents in an electrically conducting sample. Eddy currents in the sample generate a secondary magnetic field that opposes the primary field produced by the excitation coil. In reaction to a pulse excitation field, the secondary field exhibits a decaying exponential signature with a time constant proportional to the sample conductivity. The declining exponential profile, which can be used to determine the extent of corrosion in the sample, is influenced by the thickness, conductivity, and permeability of the sample, as well as the distance of the sample from the sensing element (lift-off). PEC has long been used to detect corrosion in both oil and gas pipelines and water pipes [23]–[26] and reinforced concrete structures [27]–[29]. Due to the large frequency range of the excitation signal, PEC is the most adaptive and frequent NDE method for checking ferromagnetic materials, because it can find flaws deep within the test material. The area under the curve (AUC) for the magnetic field sensor output time-series in response to the secondary magnetic field was recently demonstrated by us to be an effective feature for corrosion assessment [29].

In this paper, we have compared the performance of EMI and PEC based techniques to detect incipient corrosion of sacrificial anodes. Experimental measurements were performed with an impressed-current based accelerated corrosion system for in-situ evaluation of the RMSD of the conductance spectra of the PZT transducer attached to the sacrificial anode and AUC feature for the PEC sensor (illustration of experiment shown in Figure 1). We demonstrate that the EMI measurement is highly sensitive to initial corrosion in the anode, with sensitivity reducing over the duration of the experiment as the anode is progressively corroded due to delamination of corrosion by-products. In contrast, the PEC method shows excellent linearity over the duration of the experiment, with the sensitivity not affected by delamination of corrosion by-products. The experimental observations show excellent agreement with finite element method (FEM) simulations performed in COMSOL Multiphysics. A key insight obtained from the work presented here is that it is possible to effectively monitor the degradation of sacrificial anodes by operating both sensors in tandem, using EMI signature for identifying incipient and early-stage corrosion, and utilizing the excellent linearity of PEC for estimating extent of corrosion over prolonged duration. If the application requires monitoring of state of health of the anodes for a long time, PEC provides a direct measurement of extent of corrosion, with no post-processing needed. Our work also opens up the possibility of exploring PEC as an non-destructive evaluation (NDE) technique for on-demand and real-time monitoring of sacrificial anodes in structures such as ships, wherein EMI measurements may be prohibited due to lack of electrical access to the PZT transducer on anodes affixed on the external surface of the ship.

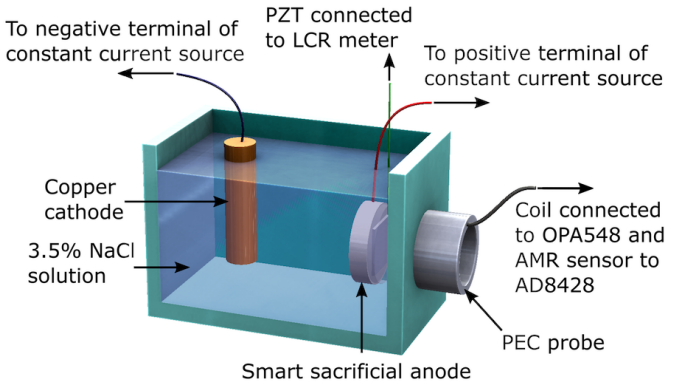

Fig. 1. Schematic of the experimental setup used for characterization of corrosion of sacrificial anode with EMI and PEC measurements.

II. Experimental Setup

A. PEC Probe

Figure 2(a) shows all the components of the sensing assembly and their placements. The 3D printed holder houses two coils used for exciting eddy current in the sample, and an AMR sensor (Honeywell HMC1001) for detecting the field produced due to the eddy currents. Unlike PEC probes that use coils to detect change in the magnetic flux, the AMR sensor presents a response proportional to the magnetic field magnitude. A solid cylindrical holder with a vertical slot designed to the dimensions of the AMR sensor was made into which the sensor can be inserted. Copper wire of diameter 0.05 cm was wound on

TABLE I
PARAMETERS FOR TRANSMISSION AND CANCELLATION COILS

Parameter	Transmission coil	Cancellation coil
Resistance	$0.4\,\Omega$	$0.1\,\Omega$
Inductance	$40\,\mu$H	$7.5\,\mu$H
Outer diameter	2.5 cm	1.5 cm
Length of solenoid (L)	2.5 cm	1.39 cm
Number of turns (N)	45	25
Turns-to-length ratio (N/L)	$1800\,\mathrm{m}^{-1}$	$1800\,\mathrm{m}^{-1}$

this cylinder (denoted as 'cancellation coil' in Figure 2(a)). This coil and sensor assembly was inserted into a larger hollow cylinder on which another coil was wound (denoted as 'transmission coil' in Figure 2(a)). This sub-assembly was then placed inside an external holder with a cylindrical cavity and square base ensuring that the sensitive axis of the AMR sensor was aligned with the axis of the two concentric coils by holding the entire sub-assembly rigidly in place. The net magnetic field at the AMR sensor due to both coils can be canceled by causing current to flow in clockwise direction in one coil and counter-clockwise direction in the other, and carefully adjusting their magnitudes to be equal. This helps in reducing the AMR output offset voltage in absence of a sample in the vicinity of the sensor. This method of compensating the offset voltage of the AMR sensor enables detection of small changes in the sensor output due to magnetic fields induced by the eddy currents in the conducting sample. Since the magnetic field inside a solenoid coil is directly proportional to its turns-to-length ratio, this ratio was kept the same by design for both coils to achieve magnetic field cancellation at the AMR sensor in absence of any external magnetic field. The parameters of interest for the transmission coil and cancellation coil are tabulated in Table I. The coil current was adjusted to be 200 mA. A high current operational amplifier (Texas Instruments OPA548) was used in non-inverting amplifier configuration with gain $=2$ to drive the current in the coils. The circuit design for the OPA548 stage is based on coil excitation circuit reported by Ulapane *et al.* [30]. The differential output of the HMC1001 was amplified using an ultra-low noise instrumentation amplifier (Analog Devices AD8428) with gain $=2000$. The excitation pulse was generated using an arbitrary function generator (Tektronix AFG31052), and an oscilloscope (Keysight DSOX2014A) was used to record the excitation pulse and sensor output.

B. Smart Sacrificial Anode

The smart sacrificial anode was manufactured with the process described in our previous work [6]. It comprises of a commercially available cylindrical zinc sacrificial anode (Canode, Krishna Conchem Products Pvt. Ltd.) of diameter 3.6 cm and thickness 0.73 cm, instrumented with PZT-5H transducer of dimensions $20 \times 20 \times 0.4\text{mm}^3$ (SP-5H, Sparkler Ceramics Pvt. Ltd.). A photograph of the assembly is shown in Figure 2(b). The surface of the zinc anode to which the PZT transducer is to be attached was first gently polished with fine grit sandpaper. The PZT transducer was affixed on the center of the polished side with Fewikwik® instant adhesive, and then a coating of waterproofing epoxy (M-Seal® Clear RTV

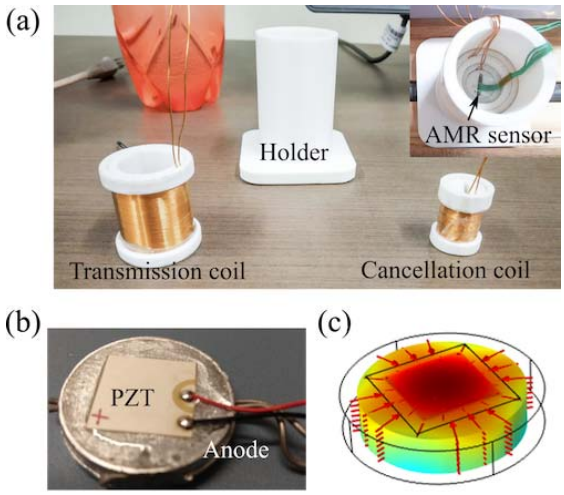

Fig. 2. (a) PEC sensor assembly consisting of a 3D printed holder, two co-axial coils and AMR sensor that fit within each other. Inset: integrated PEC probe, showing the transmission and cancellation coils assembled within the holder, with the AMR sensor inserted in the slot inside the cancellation coil. (b) Photograph of the PZT transducer bonded to zinc sacrificial anode. (c) Mode shape of the radial expansion mode of the structure analyzed for EMI measurements.

Silicone Sealant) was applied over the PZT transducer. This waterproofing sealant protects the PZT transducer from the liquid electrolyte used in the accelerated corrosion experiment, and also protects the polished surface of the anode from corroding. The assembly was left undisturbed for 12 h to allow the epoxy to cure. The impedance of the PZT transducer corresponding to radial mode of expansion of the structure (Figure 2(c)) was measured using a precision LCR meter (Agilent E4980A). The LCR meter was connected to a computer via USB, and controlled using a custom-made software designed with LabVIEW for data acquisition. The impedance recordings were used to compute RMSD of the conductance spectra, that was used to quantify the damage index i.e. extent of corrosion. RMSD of the EMI signature has been shown to be a reliable indicator of change in material parameters due to corrosion [16]. RMSD (%) is expressed as [14]–[16]:

$$\text{RMSD}\ (\%) = \sqrt{\frac{\sum_{i=1}^{N}\left(G_i^1 - G_i^0\right)^2}{\sum_{i=1}^{N}\left(G_i^0\right)^2}} \times 100 \qquad (1)$$

where G_i^0 is the baseline conductance value and G_i^1 is the post corrosion conductance value at frequency index i, corresponding to N frequency points in a given frequency range $[f_{start}, f_{end}]$, where f_{start} corresponds to index $i = 1$ and f_{end} corresponds to index $i = N$.

C. Accelerated Corrosion Setup

The experimental setup for accelerated corrosion by means of applied impressed current consisted of an electrolytic cell with a set of two electrodes submerged in an electrolyte [6]. We used a copper tube as cathode and 3.5% NaCl solution as electrolyte. The copper electrode was connected to negative terminal of a constant current source (Aplab LQ6324T) while positive terminal of the current source was connected to the zinc anode assembly. The PEC probe was affixed on the

Fig. 3. Experimental set-up showing the position of the sacrificial anode with PZT transducer and the PEC probe fixed externally.

exterior surface of the cell container, such that the axis of the excitation coils within the PEC probe coincided with the axis of the cylindrical sacrificial anode. A photograph of this assembly is shown in Figure 3. The constant current source supplies current of magnitude 0.35 A. After every 30 min interval, the current source was turned off and electromechanical impedance and PEC sensor output were recorded, without disturbing the mechanical arrangement of the apparatus. The experiment was performed for a maximum duration of 210 min.

III. Finite Element Simulation Models

A. EMI FE Model

To study the corrosion induced variation in RMSD, the zinc anode instrumented with PZT transducer was modeled in a commercially available FE software (COMSOL Multiphysics). To reduce the computational complexity, we set up a 2D axisymmetric model (Figure 4). For the 2D axisymmetric analysis, the square shaped PZT transducer was modeled as an equivalent circular shaped transducer with radius r_T [6]:

$$r_T = L\frac{\beta_T}{\pi} \tag{2}$$

where $L = 20$ mm denotes the edge length of the square PZT transducer, β_T is the dimensionless frequency parameter obtained by solving the characteristic equation $\beta_T J_0(\beta_T) - (1-\nu_T)J_1(\beta_T) = 0$, where J_0 and J_1 are the Bessel functions of first kind of order 0 and 1, respectively [31], and ν_T denotes the Poisson's ratio of the transducer material (PZT). The system used in this experiment thus corresponds to an equivalent circular PZT transducer with radius 13 mm [6].

The conversion of zinc to zinc oxide is governed by the chemical reaction: $Zn + 0.5\,O_2 \xrightarrow{ZnO}$. The amount of mass loss in zinc due to corrosion is depicted by Faraday's law:

$$\Delta m_{Zn} = \frac{IMt}{Fz} \tag{3}$$

where Δm_{Zn} is the mass loss of zinc, $I = 0.35$ A is current passing through the cell (impressed current in accelerated corrosion experiment), M is molecular weight of the reactive species (zinc), t is total time duration for which current flows in the cell (corrosion time), $F = 96485\,\mathrm{C\ mol^{-1}}$ is Faraday's constant, and $z = 2$ is valency of the reactive species (zinc). Mass loss of 1 g of zinc produces 1.24 g of zinc oxide. We assume that the radius of the disk shaped anode ($R = 1.8$ cm) does not change due to corrosion, since the bottom circular face undergoes significantly higher corrosion due to its larger surface area as compared to the side walls, and due to waterproofing of the top circular face of the anode in the experiment. Therefore, reduction of thickness of zinc layer by 1 cm results in formation of 1.57 cm of zinc oxide. Table II lists the material properties for zinc and zinc oxide used for these calculations. We thus obtain following expression for thickness of zinc oxide layer $h(t)$:

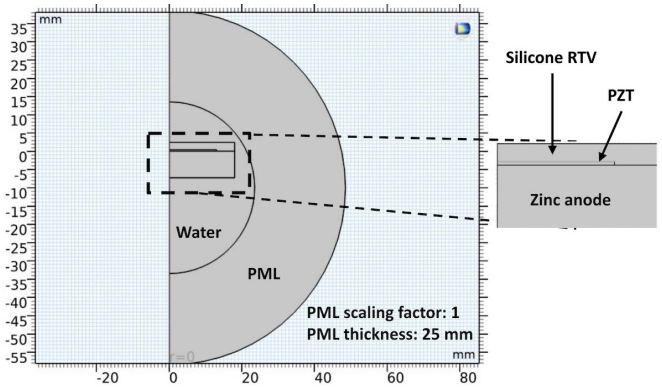

Fig. 4. FE simulation set-up for EMI based sensing.

TABLE II
Material Properties Used for Calculating Mass Conversion of Zinc to Zinc Oxide

Material	Density [g/cm^3]	Molecular weight [g mol^{-1}]
Zinc	7.14	65.38
Zinc oxide	5.68	81.38

$$h(t) = \frac{1.24 \times \Delta m_{Zn}}{\pi R^2 \rho_{ZnO}} \tag{4}$$

where ρ_{ZnO} is the density of zinc oxide. We have previously established that the degradation of the sacrificial anode during corrosion is attributed to conversion of zinc to zinc oxide, and partial delamination of zinc oxide (corrosion by-product) [6]. The delamination was characterized using a parameter termed as the non-delaminated factor Γ_d, which is the ratio of the actual (non-delaminated) thickness of zinc oxide layer that remains on the anode $h_d(t)$, to the total thickness of the zinc oxide layer in absence of delamination $h(t)$:

$$\Gamma_d(t) = \frac{h_d(t)}{h(t)} = 1 - C_1 t^A + C_2 t^{2A} \tag{5}$$

where C_1 and C_2 are reaction dependent constants. Parameters A, C_1 and C_2 are empirically determined, and accordingly the geometry is updated in the FE model for increasing values of corrosion time (t).

Since the anode is immersed in 3.5% NaCl solution in the experiment, the liquid introduces damping in the EMI of the anode-PZT system. Perfectly matched layer (PML) was used to introduce this damping in the FE model for *frequency domain* study, to obtain the EMI spectra. The PML thickness and scaling factor were set as 25 mm and 1, respectively. The mesh settings for the PML layer were as follows: mapped-mesh, with 5.5 mm element size. Other domains in the model (anode, PZT, silicone RTV and the surrounding water medium) were modeled with free triangular mesh with 4.7 μm element size.

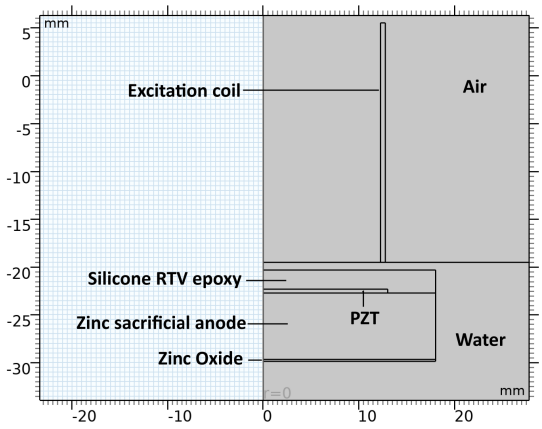

Fig. 5. FE simulation set-up for PEC based sensing.

B. PEC FE Model

Since the sacrificial anode (with equivalent circular PZT transducer) as well as the coils are cylindrical in shape, the PEC set-up was also modelled using 2D axisymmetric geometry to reduce the computation time. Figure 5 shows the geometry set up in the FE simulation. The sacrificial anode is modelled in water environment while the cylindrical coil is modelled with air as the surrounding medium, to mimic the experimental conditions. The plastic container will not have any impact on the PEC signal being made of a non-magnetic material, and is therefore not incorporated in the FE model. We observed that the AMR sensor was sensitive to corrosion of the anode even when operated using only the transmission coil (i.e. the cancellation coil was disconnected and not used). Therefore, we modelled only the transmission coil in the FE model for comparison against experimental results. The thicknesses of zinc and zinc oxide layers for increasing duration of applied impressed current are calculated using equation (5), and accordingly updated in the model. We solved for the electromagnetic fields using *AC/DC module* in COMSOL Multiphysics. *Extremely fine* mesh setting was used for physics-controlled mesh. To visualize the magnetic field at the location of the AMR sensor in the PEC sensor assembly, a point probe (monitor) for magnetic flux density was added to the FE model A square wave function of amplitude 1 V and pulse width 1 ms was applied to the coil as excitation voltage (pulse). The monitor recorded the magnetic flux density, which has contributions from field generated by the transmission coil, as well as secondary magnetic field generated by induced eddy currents in the sacrificial anode, with 5 μs time-step.

IV. Results and Discussion

In our previous work, we estimated the extent of corrosion of the sacrificial anode by analyzing the shift in peak frequency observed in the susceptance spectra of the PZT transducer [6]. Estimating change in geometric properties of the anode based on frequency shift requires high quality factor electromechanical resonance, and assembly of the anode in such a manner that the damping in the system is minimized. In this work, the anode is nestled against the wall of the plastic container to be in close vicinity of the PEC probe, and this assembly introduces significant damping in the electromechanical resonance and makes it difficult to estimate the peak frequency (Figure 6). Therefore, we examined the variation in RMSD (%) of the conductance spectra due to corrosion in the anode on account of impressed current. Figure 7(a) shows representative conductance spectra obtained

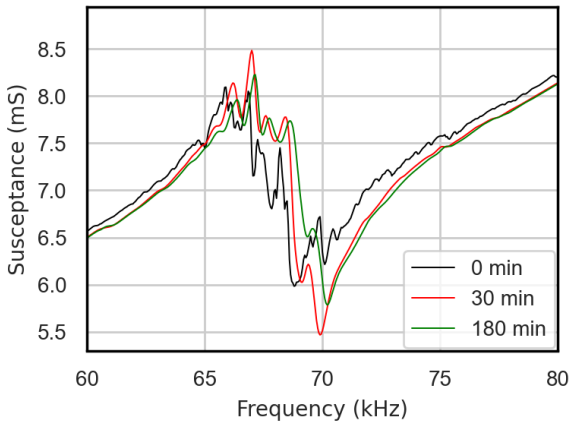

Fig. 6. Susceptance spectra acquired from PZT transducer for experimental setup shown in Figure 3. Due to damping introduced by the arrangement of the anode, it is difficult to discern the peak frequency for the electromechanical resonance.

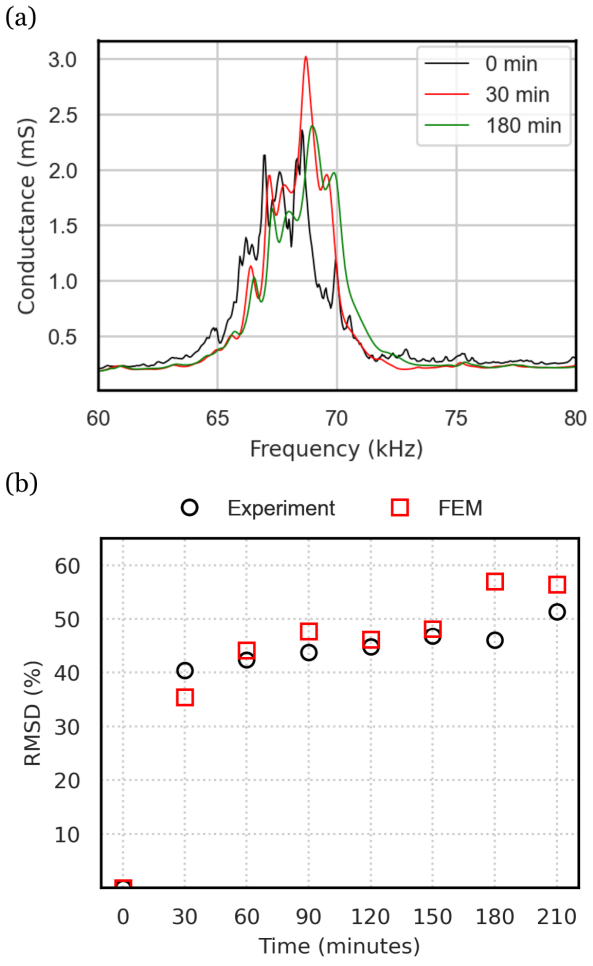

Fig. 7. (a) Representative conductance spectra acquired from PZT transducer. (b) Comparison of FE model and experimental results for RMSD (%) of conductance spectra for increasing duration of applied impressed current.

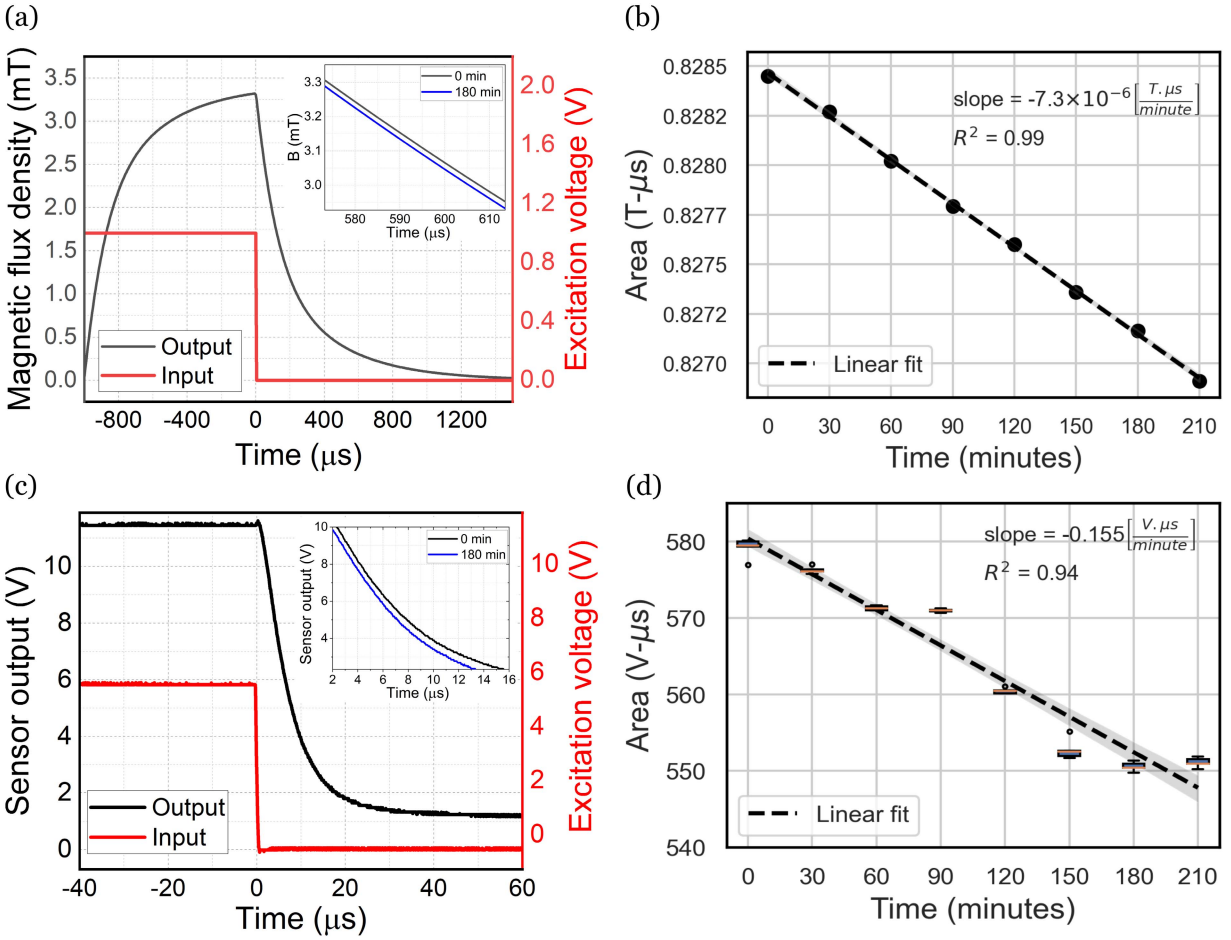

Fig. 8. (a) Input PEC pulse and signal recorded by the probe (monitor) in FE model. The inset shows change in the monitor signal before application of impressed current (0 min) and after application of impressed current for 180 min. (b) Variation in AUC computed from $t = 0$ μs to $t = 1500$ μs with time (for which impressed current is applied). (c) Input PEC pulse and AMR sensor output (amplified with instrumentation amplifier) obtained experimentally. The inset shows change in the instrumentation amplifier output before application of impressed current (0 min) and after application of impressed current for 180 min. (d) Variation in AUC computed from $t = 0$ μs to $t = 60$ μs with time (for which impressed current is applied).

before application of impressed current (labeled 0 min), and after applying impressed current for 30 min and 180 min. The RMSD is calculated as per the expression provided in equation (1). Based on experimental results, we obtain the following expression for non-delaminated factor:

$$\Gamma_d(t) = 1 - 0.2128\ t^{0.995} + 0.01875 t^{2\times 0.995} \quad (6)$$

The change in thickness of zinc and zinc oxide with time can thus be calculated using equation (6), and the corresponding values are shown in Table III. The RMSD computed for experimental results showed excellent agreement with simulation results obtained from the FE model described in section III-A, as seen in Figure 7(b). We observe that the RMSD signature is very sensitive to initial stages of corrosion, with a large shift noticed in the first 30 min upon application of impressed current. The variation in RMSD with increasing duration of applied impressed current gradually reduces beyond 30 min due to delamination of the corrosion by-products, thus showing highly nonlinear response.

For analysis of the PEC probe sensor output, we computed AUC for the time-series recorded for the monitor in FE simulation, and AMR sensor output in the experiment. Figure 8(a) shows the exponentially decaying profile for the FE simulation output (beyond 0 μs) in response to the input excitation pulse. The inset in Figure 8(a) shows variation in the curve for increasing duration of applied impressed current. The trend in AUC (computed from $t = 0$ μs to $t = 1500$ μs) with time (for which impressed current is applied) is shown in Figure 8(b). In contrast to the nonlinear response seen in RMSD obtained from EMI measurements, the AUC feature for PEC sensor shows excellent linearity with time, and therefore with extent of corrosion, with scale factor of -7.3 μT μs min^{-1} and $R^2 = 0.99$. Similar behaviour was observed for the experimental data acquired from the PEC probe. Figure 8(c) shows the AMR sensor output measured in response to the excitation pulse applied to the coil. Considering the large gain of the instrumentation amplifier AD8428 (2000) and high sensitivity of the AMR sensor (typ. 0.32 mV/V/mT as per datasheet), the output signal is clipped due to amplifier saturation for $t < 0$ μs. However, the decaying exponential profile is clearly observed upon removal of the excitation pulse at $t = 0$ μs, and the variation in the signal with increasing time of applied impressed current is seen in Figure 8(c). The trend in AUC (computed from $t = 0$ μs to $t = 60$ μs) with time (for which impressed current is applied) is shown in Figure 8(d). Each box (obtained every 30 min) in the box-plot shown

TABLE III
CALCULATED THICKNESS OF ZINC LAYER AND THICKNESS ADDED IN ZINC OXIDE LAYER FOR INCREASING CORROSION TIME

Time [min]	Zn thickness [mm]	ZnO thickness gain $h_d(t)$ [mm]
0	7.3	0
30	7.270	0.041
60	7.241	0.074
90	7.211	0.099
120	7.182	0.119
150	7.153	0.135
180	7.123	0.147
210	7.094	0.157

in Figure 8(d) corresponds to 5 separate measurements. Note that the time scales for computation of AUC are significantly different as compared to the FE model, since the FE model does not account for noise in the system, while the signal floor in AMR sensor output observed in experimental result is limited by noise in the signal chain. The AUC feature shows excellent linearity for experimental data as well, with scale factor of $-0.155\,\mathrm{V}\ \mu\mathrm{s\,min}^{-1}$ and $R^2 = 0.94$. The PEC sensor response depends on the thickness of the conducting zinc anode, and is not expected to be significantly impacted by the thickness of the dielectric zinc oxide layer. The thickness of zinc layer decreases linearly with time, in accordance with equation (3), and therefore the PEC sensor is expected to show excellent linearity with respect to corrosion time in the accelerated corrosion experiment. Note that the performance parameters reported are specific to the experimental specimen used in this study, and may vary subject to the scenario and calibration for different experimental set up and specimens. In our experiment, the total mass loss of the anode was approximately 3%. In practical applications, the critical mass loss is dependent on the design parameters of the anode: design lifetime and anode utilization factor. The anode utilization factor usually ranges between 0.8 and 0.9, indicating what fraction of mass of the anode can be consumed before it should be replaced [32]. This indicates that the method presented in our work could be used across a wide range of applications ranging from detection of early onset of corrosion to monitoring the anode for its entire service life.

V. CONCLUSION AND FUTURE WORK

In summary, we have presented comparative assessment of corrosion monitoring in sacrificial anodes using EMI and PEC sensors. Our observations indicate following salient features:

- RMSD of conductance spectra obtained from EMI signature is extremely sensitive to initial corrosion of the anode, exhibiting a sharp increase at onset of corrosion. The sensitivity gradually reduces with increasing extent of corrosion due to delamination of corrosion by-products.
- PEC sensor shows excellent linearity over entire duration of the experiment, and is a reliable and convenient tool for estimating extent of degradation of anode due to prolonged corrosion.

These observations were corroborated through FE simulations, that show excellent agreement with trends observed in the experiments. The results presented in this article establish that EMI measurements are very useful for identifying incipient corrosion, and direct measurement of corrosion dynamics such as formation and delamination of byproducts. Estimating the extent of corrosion over prolonged duration requires post-processing the results (e.g. by empirically establishing the delamination trend through equation (6)), or utilizing multiple resonances of the structure in absence of substantial damping [12]. On the other hand, PEC requires no post-processing and could potentially be used in applications such as real-time monitoring of health of sacrificial anodes in structures such as ships, wherein EMI measurements may be prohibited since the anodes are affixed on the external surface of the ship body and access to the PZT terminals may therefore not be possible. A PEC probe can be attached on the interior wall of the ship body for interrogating the anode in such an application. However, this will pose a challenge not encountered in this work, since the boundary between the PEC probe and the anode could be a conductive material that will also support eddy currents, if the ship body is constructed from steel. Our future work will focus on evaluating the suitability of utilizing PEC probes in such use cases, to monitor corrosion in an object separated from the probe with a barrier made from conductive material. Another direction we plan to explore is miniaturization of the PEC probe using planar coils and flexible PCBs, so that the probe can be adhesively attached directly on the anode in a manner similar to the method used for the PZT transducer, for applications where real-time monitoring of anodes embedded in concrete may be desirable.

ACKNOWLEDGMENT

The authors would like to thank Jeslin Thalapil and Jinit Patil at IIT Bombay for assistance with FE analysis and instrumentation. They would also like to thank Mahesh Bhaganagare, Maheshwar Mangat, Ms. Varsha Ingle, and Ms. Rabiya Kunhayi at the Wadhwani Electronics Laboratory (WEL), Department of Electrical Engineering, IIT Bombay for assistance with component procurement and PCB design and assembly.

REFERENCES

[1] L. Bertolini, M. Gastaldi, M. Pedeferri, and E. Redaelli, "Prevention of steel corrosion in concrete exposed to seawater with submerged sacrificial anodes," *Corrosion Sci.*, vol. 44, no. 7, pp. 1497–1513, Jul. 2002.

[2] V. Cicek, *Cathodic Protection: Industrial Solutions for Protecting Against Corrosion*. Hoboken, NJ, USA: Wiley, 2013.

[3] P. Astuti, R. S. Rafdinal, H. Hamada, Y. Sagawa, D. Yamamoto, and K. Kamarulzaman, "Effectiveness of rusted and non-rusted reinforcing bar protected by sacrificial anode cathodic protection in repaired patch concrete," *IOP Conf. Ser., Earth Environ. Sci.*, vol. 366, no. 1, Nov. 2019, Art. no. 012013.

[4] U. M. Angst, "A critical review of the science and engineering of cathodic protection of steel in soil and concrete," *Corrosion*, vol. 75, no. 12, pp. 1420–1433, Dec. 2019.

[5] A. Farooq, M. Hamza, Q. Ahmed, and K. M. Deen, "Evaluating the performance of zinc and aluminum sacrificial anodes in artificial seawater," *Electrochim. Acta*, vol. 314, pp. 135–141, Aug. 2019.

[6] D. Tamhane, J. Thalapil, S. Banerjee, and S. Tallur, "Smart cathodic protection system for real-time quantitative assessment of corrosion of sacrificial anode based on electro-mechanical impedance (EMI)," *IEEE Access*, vol. 9, pp. 12230–12240, 2021.

[7] E. S. de Freitas, F. G. Baptista, D. E. Budoya, and B. A. de Castro, "Equivalent circuit of piezoelectric diaphragms for impedance-based structural health monitoring applications," *IEEE Sensors J.*, vol. 17, no. 17, pp. 5537–5546, Sep. 2017.
[8] C. Zhang, G. P. Panda, Q. Yan, W. Zhang, C. Vipulanandan, and G. Song, "Monitoring early-age hydration and setting of Portland cement paste by piezoelectric transducers via electromechanical impedance method," *Construct. Building Mater.*, vol. 258, Oct. 2020, Art. no. 120348.
[9] V. Talakokula *et al.*, "Diagnosis of carbonation induced corrosion initiation and progression in reinforced concrete structures using piezo-impedance transducers," *Sens. Actuators A, Phys.*, vol. 242, pp. 79–91, May 2016.
[10] J. Wang, W. Li, C. Lan, P. Wei, and W. Luo, "Electromechanical impedance instrumented piezoelectric ring for pipe corrosion and bearing wear monitoring: A proof-of-concept study," *Sens. Actuators A, Phys.*, vol. 315, Nov. 2020, Art. no. 112276.
[11] T. Jiang *et al.*, "Monitoring of corrosion-induced degradation in pre-stressed concrete structure using embedded piezoceramic-based transducers," *IEEE Sensors J.*, vol. 17, no. 18, pp. 5823–5830, Sep. 2017.
[12] J. Thalapil, D. Tamhane, S. Banerjee, and S. Tallur, "Vibration-based inverse graphical technique for thickness estimation of bulk acoustic wave (BAW) resonators: Application for corrosion monitoring of sacrificial anodes," *Smart Mater. Struct.*, vol. 30, no. 5, May 2021, Art. no. 055015.
[13] J. Thalapil, D. Tamhane, S. Banerjee, and S. Tallur, "Corrosion monitoring of sacrificial anodes based on contour plot analysis of electro-mechanical impedance spectra," in *Proc. 21st Int. Conf. Solid-State Sens., Actuators Microsyst. (Transducers)*, Jun. 2021, pp. 1182–1185.
[14] R. Tawie and H. K. Lee, "Monitoring the strength development in concrete by EMI sensing technique," *Construct. Building Mater.*, vol. 24, no. 9, pp. 1746–1753, Sep. 2010.
[15] E. Ghafari, Y. Yuan, C. Wu, T. Nantung, and N. Lu, "Evaluation the compressive strength of the cement paste blended with supplementary cementitious materials using a piezoelectric-based sensor," *Construct. Building Mater.*, vol. 171, pp. 504–510, May 2018.
[16] V. Talakokula and S. Bhalla, "Reinforcement corrosion assessment capability of surface bonded and embedded piezo sensors for reinforced concrete structures," *J. Intell. Mater. Syst. Struct.*, vol. 26, no. 17, pp. 2304–2313, Nov. 2015.
[17] X. Chen and X. Liu, "Pulsed eddy current-based method for electromagnetic parameters of ferromagnetic materials," *IEEE Sensors J.*, vol. 21, no. 5, pp. 6376–6383, Mar. 2021.
[18] A. Fahim, P. Ghods, O. B. Isgor, and M. D. A. Thomas, "A critical examination of corrosion rate measurement techniques applied to reinforcing steel in concrete," *Mater. Corrosion*, vol. 69, no. 12, pp. 1784–1799, Dec. 2018.
[19] I. Mukherjee, J. Patil, S. Banerjee, and S. Tallur, "Phase-sensitive detection of extent of corrosion using anisotropic magnetoresistive (AMR) sensor in steel reinforcing bars (rebars)," in *Advances in Non-Destructive Evaluation*. Singapore: Springer, 2021, pp. 19–26.
[20] D. Tamhane, S. Banerjee, and S. Tallur, "Non-invasive detection of extent of corrosion in steel reinforcing bars by magnetic force measurement," in *Advances in Non-Destructive Evaluation*. Singapore: Springer, 2021, pp. 11–17.
[21] F. Nafiah *et al.*, "Parameter analysis of pulsed eddy current sensor using principal component analysis," *IEEE Sensors J.*, vol. 21, no. 5, pp. 6897–6903, Mar. 2021.
[22] M. Pan, Y. He, G. Tian, D. Chen, and F. Luo, "PEC frequency band selection for locating defects in two-layer aircraft structures with air gap variations," *IEEE Trans. Instrum. Meas.*, vol. 62, no. 10, pp. 2849–2856, Oct. 2013.
[23] L. Nguyen and J. V. Miro, "Efficient evaluation of remaining wall thickness in corroded water pipes using pulsed eddy current data," *IEEE Sensors J.*, vol. 20, no. 23, pp. 14465–14473, Dec. 2020.
[24] Z. Chu, Z. Jiang, Z. Mao, Y. Shen, J. Gao, and S. Dong, "Low-power eddy current detection with 1–1 type magnetoelectric sensor for pipeline cracks monitoring," *Sens. Actuators A, Phys.*, vol. 318, Feb. 2021, Art. no. 112496.
[25] N. Ulapane, K. Thiyagarajan, J. V. Miro, and S. Kodagoda, "Surface representation of pulsed eddy current sensor signals for improved ferromagnetic material thickness quantification," *IEEE Sensors J.*, vol. 21, no. 4, pp. 5413–5422, Feb. 2021.
[26] J. Valls Miro, N. Ulapane, L. Shi, D. Hunt, and M. Behrens, "Robotic pipeline wall thickness evaluation for dense nondestructive testing inspection," *J. Field Robot.*, vol. 35, no. 8, pp. 1293–1310, Dec. 2018.
[27] N. Ulapane, S. Wickramanayake, and S. Kodagoda, "Pulsed eddy current sensing for condition assessment of reinforced concrete," in *Proc. 14th IEEE Conf. Ind. Electron. Appl. (ICIEA)*, Jun. 2019, pp. 1–6.
[28] I. C. Eddy, P. R. Underhill, J. Morelli, and T. W. Krause, "Pulsed eddy current response to liftoff in different sizes of concrete embedded rebar," in *Proc. IEEE SENSORS*, Oct. 2019, pp. 1–4.
[29] D. Tamhane, J. Patil, S. Banerjee, and S. Tallur, "Feature engineering of time-domain signals based on principal component analysis for rebar corrosion assessment using pulse eddy current," *IEEE Sensors J.*, vol. 21, no. 19, pp. 22086–22093, Oct. 2021.
[30] N. Ulapane, A. Alempijevic, T. V. Calleja, and J. V. Miro, "Pulsed eddy current sensing for critical pipe condition assessment," *Sensors*, vol. 17, no. 10, p. 2208, Sep. 2017.
[31] V. Giurgiutiu, *Structural Health Monitoring With Piezoelectric Wafer Active Sensors*, 2nd ed. New York, NY, USA: Academic, 2014.
[32] *Recommended Practice DNV-RP-B401, Cathodic Protection Design*, document DNV-RP-B401, 2010.

Durgesh Tamhane received the M.Sc. degree in physics from the University of Mumbai, Mumbai, India, in 2011. He is pursuing the Ph.D. degree with the Department of Electrical Engineering, IIT Bombay. His thesis research focuses on design and development of sensors for structural health monitoring. He worked as a Project Research Assistant at NMPF, Department of Electrical Engineering, IIT Bombay, from 2015 to 2017. He has won the IEEE International Sensors and Measurement Student Contest Award from 2018 and 2019 IEEE Sensors Conferences. He has also received Excellence in Teaching Assistantship recognition for EE617 Sensors in Instrumentation, EE783 Advanced Semiconductor Devices Laboratory, and EE701 Introduction to MEMS courses at IIT Bombay.

Sauvik Banerjee is a Professor of Structural Engineering with the Department of Civil Engineering, IIT Bombay. Prior to joining IIT Bombay, he was an Assistant Professor at the Parks College of Engineering, Aviation and Technology, Saint Louis University, St. Louis, MO, USA. He has more than 100 publications and several awards. He has been PI for several sponsored research and industrial consultancy projects worth over U.S. $ 2 million. His research interests include SHM using wave propagation and vibration-based approaches, ultrasonic NDE of materials, and elastodynamic modeling of advanced composite structures.

Siddharth Tallur received the B.Tech. degree in electrical engineering from IIT Bombay in 2008, and the M.S. and Ph.D. degrees in electrical and computer engineering from Cornell University in 2011 and 2013, respectively. From 2013 to 2016, he worked at Analog Devices Inc., Wilmington, MA, USA, as a MEMS Products and Applications Engineer. He is an Associate Professor with the Department of Electrical Engineering, IIT Bombay. His research interests include high resolution and low cost physical and biosensors, and high-speed instrumentation and embedded systems for sensing applications.